

NAICS-Aware Graph Neural Networks for Large-Scale POI Co-visitation Prediction: A Multi-Modal Dataset and Methodology

YAZEED ALRUBYLI, Prince Sultan University, Saudi Arabia and Università di Bologna, Italy

OMAR ALOMEIR, Prince Sultan University, Saudi Arabia

ABRAR WAFA, Prince Sultan University, Saudi Arabia

DIÁNA HIDVÉGI, Intelmatix, Saudi Arabia

HEND ALRASHEED, Massachusetts Institute of Technology, USA

MOHSEN BAHRAMI, Massachusetts Institute of Technology, USA

Understanding where people go after visiting one business is crucial for urban planning, retail analytics, and location-based services. However, predicting these co-visitation patterns across millions of venues remains challenging due to extreme data sparsity and the complex interplay between spatial proximity and business relationships. Traditional approaches using only geographic distance fail to capture why coffee shops attract different customer flows than fine dining restaurants, even when co-located. We introduce NAICS-aware GraphSAGE, a novel graph neural network that integrates business taxonomy knowledge through learnable embeddings to predict population-scale co-visitation patterns. Our key insight is that business semantics—captured through detailed industry codes—provide crucial signals that pure spatial models cannot explain. The approach scales to massive datasets (4.2 billion potential venue pairs) through efficient state-wise decomposition while combining spatial, temporal, and socioeconomic features in an end-to-end framework. Evaluated on our POI-Graph dataset comprising 94.9 million co-visitation records across 92,486 brands and 48 US states, our method achieves significant improvements over state-of-the-art baselines: R^2 increases from 0.243 to 0.625 (157% improvement), with strong gains in ranking quality (32% improvement in NDCG@10).

CCS Concepts: • Computing methodologies → Neural networks; • Information systems → Spatial-temporal systems; Location based services; Recommender systems; • Applied computing → Forecasting.

Additional Key Words and Phrases: Co-visitation prediction, Graph Neural Networks, Site Selection, Market Potential Estimation, Spatial-temporal modeling, Edge regression, POI recommendation, Urban mobility, Business taxonomy embeddings, Multi-modal learning, Socioeconomic context

1 Introduction

The rapid adoption of location-enabled mobile devices has created unprecedented opportunities to analyze population-scale movement between Points-of-Interest (POIs). Such data underpins applications from urban resilience and pandemic response [18] to retail analytics [9] and next-POI recommendation [34]. In many scenarios, the critical primitive is not an isolated visit, but a *co-visitation event*: two venues visited by the same user within a short temporal window. Accurate co-visitation forecasts can directly benefit demand-aware marketing, multi-stop itinerary planning, and infrastructure investment analysis.

Predicting co-visitation patterns across the United States presents formidable challenges: with over 92,000 brands and 276 business categories, the potential co-visitation space contains 4.2 billion brand pairs. Empirical analysis reveals extreme sparsity—over 99.9% of brand pairs exhibit zero co-visits monthly, while observed pairs span five orders of

Authors' Contact Information: Yazeed Alrabyli, Prince Sultan University, Riyadh, Saudi Arabia and Università di Bologna, Bologna, Italy, yazeednaif.alrabyli2@unibo.it; Omar Alomeir, Prince Sultan University, Riyadh, Saudi Arabia, oalomeir@psu.edu.sa; Abrar Wafa, Prince Sultan University, Riyadh, Saudi Arabia, awafa@psu.edu.sa; Diána Hidvégi, Intelmatix, Riyadh, Saudi Arabia, dia.h@intelmatix.ai; Hend Alrasheed, Massachusetts Institute of Technology, Cambridge, Massachusetts, USA, hrasheed@mit.edu; Mohsen Bahrami, Massachusetts Institute of Technology, Cambridge, Massachusetts, USA, bahrami@mit.edu.

magnitude in intensity (1 to 28,000+ monthly interactions). This creates a "needle in haystack" problem where traditional collaborative filtering approaches fail. Consider predicting co-visits between a Starbucks and nearby restaurants in Manhattan. Traditional approaches using only geographic proximity miss crucial business semantics: coffee shops exhibit high complementarity with fast-casual dining (due to meal timing) but low complementarity with fine dining (different customer occasions). Capturing these nuanced relationships requires understanding both spatial proximity and semantic complementarity—precisely what business taxonomy integration provides.

Accurate co-visit prediction enables transformative applications across domains. In retail analytics, it helps optimize store placement by identifying complementary business clusters, with major chains reporting 15–25% gains in site selection accuracy [1]. In urban planning, it informs mixed-use developments that increase foot traffic and local business revenue by 30–40% [20]. For economic development, it helps identify ecosystem vulnerabilities and guide strategic investment, especially during economic disruptions. In location-based services, co-visit models improve itinerary recommendations and raise user engagement by 20–35%. Specifically, co-visit prediction between points of interest (POIs) addresses several computational challenges in spatial analytics and location modeling. First, it enables efficient pre-filtering for sales prediction models by identifying areas with high co-visit connectivity, reducing the search space from millions of potential locations to those with demonstrated customer flow relationships. Second, co-visit patterns provide location recommendation signals that incorporate semantic POI relationships beyond spatial proximity, enabling more accurate site selection based on complementary venue types and market potential. Third, predicted co-visit flows can serve as features embedded into both sales and cannibalization prediction models, capturing indications for customer redistribution effects after opening at a new location, as well as attractiveness of the area. Despite its utility, co-visit forecasting remains technically challenging. Co-visit matrices are extremely sparse and subject to temporal drift due to seasonality and economic shifts. Co-visit patterns are shaped by complex interactions among geography, business function, and socio-demographics. Finally, modern datasets contain millions of venues and billions of candidate edges, making classical methods computationally infeasible [30].

Graph Neural Networks (GNNs) provide a principled framework to combine rich node/edge attributes with topological structure. Recent GNN-based POI models have evolved rapidly [26, 32, 33], but they largely focus on individual user behavior through node-level prediction tasks rather than population-level co-visit forecasting through edge-regression. Moreover, they seldom incorporate domain-specific taxonomies like NAICS that are critical for interpretability [8, 41]. In this work, we cast co-visit prediction as a spatio-temporal edge-regression problem and present the first end-to-end GNN that jointly embeds NAICS codes, temporal signals, and spatial relations while scaling to hundreds of millions of POI pairs. We focus on pre-pandemic data (Jan 2018–Mar 2020) to establish robust baselines on stable behavioral patterns. Unlike existing approaches targeting individual user behavior, our method predicts population-level mobility patterns through learnable business semantics. Our contributions are twofold: (1) Methodological: We formulate POI co-visit as an edge regression task and develop a NAICS-aware GraphSAGE framework that incorporates learnable business taxonomy embeddings for population-level co-visit prediction at scale. (2) Empirical: We achieve strong predictive performance (Test R^2 of 0.625, representing a 157% improvement over the best baseline) through extensive experiments, demonstrating significant improvements over traditional spatial interaction models and existing graph-based approaches.

2 Related Work

Graph Neural Networks have emerged as powerful tools for spatial-temporal prediction due to their ability to model complex relational dependencies [3, 30]. Early spatial GNN approaches like STGCN [42] and GraphWaveNet [31]

demonstrated effectiveness for traffic flow prediction through spatial-temporal convolutions. Recent advances include ASTGCN’s adaptive adjacency learning [13], STGCN’s multi-component fusion [22], and GMAN’s spatial-temporal attention mechanisms [43].

The field has seen rapid evolution toward more sophisticated architectures. STGODE [19] introduces ordinary differential equations for continuous spatial-temporal modeling, while STGFormer [4] combines transformers with graph convolutions for improved traffic forecasting. Recent work on spatio-temporal graph learning [16] and trajectory-based prediction [21] demonstrates the growing sophistication of GNN approaches for mobility modeling.

For POI applications specifically, several architectures have shown promise: STHGCN [33] employs hypergraphs for sequential POI recommendation, GETNext [34] augments transformers with trajectory flow maps, and recent work explores multi-modal integration for location-based services [28, 32].

Existing POI-focused GNNs primarily target individual user behavior through node-level prediction tasks (next-POI recommendation, user preference modeling). In contrast, our work addresses population-level co-visitaiton forecasting through edge-regression, requiring fundamentally different modeling approaches that capture aggregate mobility patterns rather than individual preferences.

Incorporating business semantics into spatial models remains challenging. Most approaches treat business categories as simple one-hot features [10] or static embeddings [41], failing to capture semantic relationships between categories. Recent work explores BERT-based business descriptions [29] and hierarchical category relationships [35], but these approaches don’t jointly optimize business semantics with spatial-temporal patterns. Recent advances in hierarchical category-aware models [25] and business category representation learning [8, 15] demonstrate the growing importance of domain-specific taxonomy integration.

For edge-level prediction, traditional link prediction methods focus on binary connections [38], while continuous edge weight regression presents unique challenges. Recent advances include EdgeGNN’s edge-centric message passing [44] and WGCN’s weighted graph handling [40], but these methods struggle with the extreme sparsity (state-level density $< 10^{-3}$) characteristic of co-visitaiton graphs. Recent work on graph structure learning [37] and edge-level explanation [39] provides new perspectives on continuous edge weight prediction in sparse networks. Existing methods either ignore business categories entirely or treat them as static features. We introduce learnable NAICS embeddings that capture industry-specific behavioral patterns within the GNN architecture, enabling the model to discover latent business relationships relevant for co-visitaiton prediction.

Classical spatial interaction models like the gravity model provide interpretable frameworks but lack the flexibility to capture non-linear relationships and multi-modal features. Matrix factorization approaches [17] and collaborative filtering methods struggle with sparsity and cold-start problems inherent in mobility data.

Recent industrial-scale systems like PinSage [36] and MGN [24] achieve billion-edge scaling but focus on recommendation tasks rather than spatial interaction modeling. For mobility specifically, most large-scale approaches target transportation flows [31] rather than business co-visitaiton patterns. Recent advances in urban mobility analysis demonstrate the potential of multimodal data fusion [1] and contrastive learning approaches [27] for understanding complex mobility patterns. Additionally, scalable graph processing systems [5, 11] and comprehensive mobility understanding frameworks [12, 20] provide new foundations for large-scale spatial analysis.

Existing edge prediction methods face significant scalability challenges when applied to nationwide POI networks with extreme sparsity and five orders of magnitude variation in interaction strength. Our approach combines GraphSAGE’s inductive learning with domain-specific NAICS embeddings to enable effective edge regression while maintaining computational tractability.

3 Methodology

Our goal is to develop a scalable GNN-based approach for predicting population-level POI co-visitation. Let \mathcal{V} denote the set of Points of Interest (represented as brands) and \mathcal{E}_t the multiset of observed co-visitation pairs in month t . For any brand pair $(i, j) \in \mathcal{V} \times \mathcal{V}$, we define $y_{ij}^{t+\Delta}$ as the number of distinct mobile devices that visit both brands i and j within a one-hour temporal window during the prediction horizon $t + \Delta$. Given historical observations over L months, our objective is to learn a function $\hat{y}_{ij}^{t+\Delta} = f(\mathcal{G}_{t-L:t}, \mathbf{X}_{t-L:t}, \mathbf{S}_t; \Theta)$, where: $\mathcal{G}_{t-L:t} = (\mathcal{V}, \mathcal{E}_{t-L} \cup \dots \cup \mathcal{E}_t)$ is the aggregated co-visitation graph over the historical window, $\mathbf{X}_{t-L:t}$ represents the temporal sequence of node and edge features, \mathbf{S}_t captures socioeconomic context features at time t , and Θ are the learnable model parameters.

This formulation casts co-visitation prediction as a spatio-temporal edge-regression problem with highly skewed, sparse targets spanning multiple orders of magnitude.

3.1 Graph Construction and Representation

To ensure computational tractability while preserving regional mobility patterns, we decompose the nationwide co-visitation network into state-specific subgraphs. For each state s , we construct $\mathcal{G}_s = (\mathcal{V}_s, \mathcal{E}_s)$, where \mathcal{V}_s is the set of nodes, each representing a unique brand in s . The edge set \mathcal{E}_s contains undirected edges (i, j) if brands i and j exhibit co-visitation frequency above a minimum threshold (5 device traces) within the monthly aggregation window. This threshold balances graph density with statistical significance. We aggregate multiple physical locations of the same brand to create brand-level nodes, reducing noise from location-specific variations while preserving business semantic information.

The resulting state graphs exhibit diverse characteristics: large states like Texas contain $\sim 1.3M$ edges with 92K nodes, while smaller states like Vermont have $\sim 27K$ edges with fewer than 2K nodes, providing natural scale diversity for evaluation.

3.2 Multi-Modal Feature Engineering

Our feature engineering pipeline creates a rich, multi-dimensional representation spanning business semantics, spatial relationships, temporal dynamics, and socioeconomic context.

Each brand node i is represented by $\mathbf{x}_i \in \mathbb{R}^{17}$ comprising: (1) NAICS taxonomy embedding: We learn a 16-dimensional embedding $\mathbf{e}_{\text{NAICS}} \in \mathbb{R}^{16}$ for each of the 276 unique 6-digit NAICS codes in our dataset. The first embedding vector (index 0, typically reserved for padding or unknown tokens) is initialized to constant zero, while the remaining embeddings use PyTorch's default initialization. These embeddings are learned end-to-end, allowing the model to discover latent business category relationships relevant for co-visitation prediction. The embedding dimension is chosen to balance expressiveness with parameter efficiency. (2) Popularity score: A single scalar $p_i \in \{0, 1, 2\}$ encoding relative brand prominence within industry and geographic context, computed via state- and industry-stratified quantile analysis. Formally, the node feature vector is: $\mathbf{x}_i = [\mathbf{e}_{\text{NAICS}(i)} \| p_i] \in \mathbb{R}^{17}$.

For each brand pair (i, j) , we construct a 10-dimensional edge feature vector $\mathbf{x}_{ij} \in \mathbb{R}^{10}$, including: (1) Spatial features (1D): log-transformed great-circle distance d_{ij} between brand centroids $d_{ij}^{\text{norm}} = \frac{\log(d_{ij}+1) - \mu_d}{\sigma_d}$. (2) Temporal features (2D): Cyclical month encoding to capture seasonality: $[\sin(2\pi \cdot m/12), \cos(2\pi \cdot m/12)]$, where m is the month index. (3) Interaction features (7D): Brand popularity interactions and derived statistics:

$$[p_i + p_j, p_i \cdot p_j, |p_i - p_j|, \max(p_i, p_j), \min(p_i, p_j), \mathbb{I}_{p_i=p_j}, \sqrt{p_i \cdot p_j}]$$

We augment the feature space with 38 state-level socioeconomic indicators $\mathbf{s}_t \in \mathbb{R}^{38}$ from Census ACS and BEA data sources. These features are temporally aligned with a lag-1 strategy to reflect the delayed impact of economic conditions on mobility patterns. Socioeconomic features are integrated at the edge level during prediction based on three key insights: (1) *Regional mobility patterns*: Economic conditions affect population-level mobility more than individual preferences—unemployment rates influence restaurant co-visits across entire metropolitan areas; (2) *Computational efficiency*: State-level aggregation allows feature sharing across all edges within a state, reducing parameter overhead while capturing regional effects; (3) *Temporal stability*: Economic indicators change slowly relative to daily mobility patterns, justifying the lag-1 integration strategy to reflect delayed economic impacts on behavior.

For each edge (i, j) in state s , we concatenate the state-specific socioeconomic vector \mathbf{s}_s with the edge features before final prediction: $\mathbf{x}_{ij}^{extended} = [\mathbf{x}_{ij} \parallel \mathbf{s}_s] \in \mathbb{R}^{48}$, where $\mathbf{x}_{ij} \in \mathbb{R}^{10}$ contains spatial, temporal, and interaction features, and $\mathbf{s}_s \in \mathbb{R}^{38}$ contains state-level socioeconomic indicators. This design enables the model to condition co-visitaiton predictions on regional economic context while maintaining computational efficiency through shared state-level features. Ablation studies (Appendix A) confirm that removing socioeconomic features reduces R^2 by 18.2%, validating their importance for population-level mobility modeling.

3.3 NAICS-Aware GraphSAGE Architecture

Our model architecture extends GraphSAGE [14] with domain-specific enhancements for co-visitaiton prediction. Figure 3 in the Appendix presents the complete architectural design, illustrating how learnable NAICS business taxonomy embeddings are systematically integrated with multi-modal spatial-temporal features through a deep GraphSAGE backbone to enable scalable edge-level co-visitaiton prediction. The architecture demonstrates three key innovations: (1) domain-specific NAICS embedding initialization that captures business category semantics, (2) multi-modal feature fusion combining node embeddings with engineered edge features, and (3) a specialized prediction head designed for regression on extremely sparse co-visitaiton graphs.

The core GraphSAGE update at layer k follows:

$$\mathbf{m}_i^{(k)} = \text{AGGREGATE}^{(k)}(\{\mathbf{h}_j^{(k-1)} : j \in \mathcal{N}(i)\}) \quad (1)$$

$$\mathbf{h}_i^{(k)} = \sigma(\mathbf{W}^{(k)} \cdot [\mathbf{h}_i^{(k-1)} \parallel \mathbf{m}_i^{(k)}]) \quad (2)$$

where $\mathbf{h}_i^{(0)} = \mathbf{x}_i$, $\mathcal{N}(i)$ denotes the neighborhood of node i , \parallel represents concatenation, and we use mean aggregation:

$$\text{AGGREGATE}^{(k)} = \frac{1}{|\mathcal{N}(i)|} \sum_{j \in \mathcal{N}(i)} \mathbf{h}_j^{(k-1)} \quad (3)$$

We employ a 5-layer architecture with hidden dimension $d = 512$, providing sufficient receptive field coverage while maintaining computational efficiency. Each layer includes a linear transformation $\mathbb{R}^{d_{in}} \rightarrow \mathbb{R}^{512}$, hyperbolic tangent activation $\tanh(\cdot)$, and dropout regularization with rate $\rho = 0.2$.

We choose GraphSAGE over other GNN variants (GAT, GCN) for three key reasons validated by our problem characteristics: (1) *Inductive capability*: GraphSAGE’s sampling-based approach enables training on subgraphs and inference on unseen nodes, crucial for handling new brands or seasonal POI changes that frequently occur in mobility data; (2) *Scalability*: Fixed-size neighborhood sampling provides predictable memory usage essential for large state-level graphs—our largest graphs contain $> 1.3M$ edges with memory requirements that would be prohibitive for attention-based methods like GAT; (3) *Sparsity handling*: Mean aggregation proves empirically superior to attention mechanisms

for extremely sparse graphs (state-level density $< 10^{-3}$) where attention weights become unstable due to limited connectivity patterns.

We employ multi-layer neighbor sampling with decreasing fanout sequence [15, 10, 5] for computational efficiency and stable training. This design follows three principles: (1) *Information preservation*: Higher fanout in deeper layers (15 for layer 1) captures broader neighborhood context essential for sparse graphs; (2) *Computational tractability*: Decreasing fanout (5 for layer 5) controls memory growth, enabling training on graphs with >1M edges; (3) *Noise reduction*: Smaller fanout in final layers focuses on most relevant neighbors, reducing noise from distant, weakly connected nodes. Empirical analysis shows this sequence achieves 94% of full-neighborhood performance while reducing memory usage by 75%.

Our training procedure combines balanced mini-batch sampling with multi-layer neighborhood aggregation to handle the extreme sparsity of co-visit graphs. For each state graph, we sample balanced batches containing equal numbers of positive edges (observed co-visits) and negative edges (randomly sampled zero co-visit pairs). The NAICS embeddings are extracted and concatenated with popularity scores to form node features, which then propagate through the 5-layer GraphSAGE encoder. Edge features combine the learned node embeddings with spatial, temporal, and interaction features before final prediction. The complete training algorithm with detailed pseudo-code is provided in Appendix C.

3.3.1 Edge-Level Prediction Head. After the final GraphSAGE layer, we obtain node embeddings $\mathbf{z}_i \in \mathbb{R}^{512}$. The co-visit intensity prediction for edge (i, j) combines node embeddings with extended edge features through a carefully designed fusion architecture.

Feature fusion strategy. Rather than naive concatenation of all features, we employ a two-stage fusion approach to manage the high-dimensional feature space effectively:

$$\mathbf{f}_{\text{nodes}} = \text{ReLU}(\mathbf{W}_{\text{node}} \cdot [\mathbf{z}_i \| \mathbf{z}_j] + \mathbf{b}_{\text{node}}) \quad (4)$$

$$\mathbf{f}_{\text{edges}} = \text{ReLU}(\mathbf{W}_{\text{edge}} \cdot \mathbf{x}_{ij}^{\text{extended}} + \mathbf{b}_{\text{edge}}) \quad (5)$$

$$\hat{y}_{ij} = \mathbf{w}^{\top} \cdot [\mathbf{f}_{\text{nodes}} \| \mathbf{f}_{\text{edges}}] + b \quad (6)$$

where $\mathbf{W}_{\text{node}} \in \mathbb{R}^{256 \times 1024}$ and $\mathbf{W}_{\text{edge}} \in \mathbb{R}^{32 \times 48}$ are learned projection matrices that reduce the dimensionality while preserving relevant information. The final prediction layer operates on a more manageable 288-dimensional space (256 + 32), significantly reducing the risk of overfitting while maintaining representational capacity.

Architectural rationale. This two-stage approach offers several advantages: (1) *Dimensionality management*: Reduces the effective feature space from 1072 to 288 dimensions, improving generalization; (2) *Feature specialization*: Allows different transformation strategies for node-level and edge-level features; (3) *Computational efficiency*: Reduces the number of parameters in the final prediction layer by approximately 70%; (4) *Interpretability*: Enables separate analysis of node-level versus edge-level feature contributions.

The dimensions are chosen based on ablation studies showing that 256-dimensional node projections preserve most GraphSAGE embedding information while 32-dimensional edge projections capture essential spatial-temporal patterns without overfitting to the training data.

Prediction head. The final prediction head combines the fused features with learned weights $\mathbf{w} \in \mathbb{R}^{288}$ and bias $b \in \mathbb{R}$: $\hat{y}_{ij} = \mathbf{w}^{\top} \cdot [\mathbf{f}_{\text{nodes}} \| \mathbf{f}_{\text{edges}}] + b$.

3.4 Training Procedure and Optimization

3.4.1 *Loss Function and Negative Sampling.* We optimize mean squared error (MSE) between predictions and ground-truth co-visit counts: $\mathcal{L} = \frac{1}{|\mathcal{B}|} \sum_{(i,j) \in \mathcal{B}} (\hat{y}_{ij} - y_{ij})^2$. To address the extreme sparsity of co-visit graphs (state-level density $< 10^{-3}$), we employ balanced mini-batch training: each batch \mathcal{B} contains equal numbers of positive edges (observed co-visits) and negative edges (randomly sampled zero co-visit pairs).

3.4.2 *Optimization Details.* AdamW optimizer with learning rate $\eta = 10^{-3}$, weight decay $\lambda = 10^{-4}$, and default momentum parameters ($\beta_1 = 0.9, \beta_2 = 0.999$).

Training regime: Maximum 300 epochs with early stopping based on validation MAE (patience = 20 epochs). Learning rate decay by factor 0.5 when validation loss plateaus for 10 epochs.

Regularization: Layer-wise dropout ($\rho = 0.2$) and L2 weight decay to prevent overfitting on the relatively small number of parameters relative to the large graphs.

3.5 Evaluation Methodology

3.5.1 *Temporal Splitting Strategy.* We employ chronological data splitting to ensure realistic evaluation:

- Training: January 2018–December 2019 (24 months)
- Validation: January–February 2020 (2 months)
- Testing: March 2020 (1 month, final pre-pandemic period)

This split ensures no future information leakage and tests the model’s ability to generalize to unseen temporal patterns while maintaining focus on stable pre-pandemic mobility behaviors.

3.5.2 *Evaluation Metrics.* We report multiple complementary metrics to assess different aspects of prediction quality: Mean Absolute Error (MAE), Root Mean Square Error (RMSE), Mean Square Error (MSE), and coefficient of determination (R^2) for absolute prediction accuracy.

Normalized Discounted Cumulative Gain (NDCG@10) and Mean Reciprocal Rank (MRR) to evaluate the model’s ability to rank co-visit pairs, crucial for recommendation applications. We provide box plot visualizations of performance distributions across multiple runs to demonstrate both statistical significance and experimental consistency (Figure 1).

3.5.3 *Statistical Significance Testing.* Based on established practices for statistical evaluation in machine learning [6, 7] and accounting for variance in ML benchmarks [2], we compute statistical significance using paired t-tests. For our experimental results with $n=5$ runs, we calculate p-values using paired t-tests and report Cohen’s d effect sizes to quantify practical significance beyond statistical significance.

3.6 Computational Complexity Analysis

For a graph with N nodes and E edges, each GraphSAGE layer has complexity $O(E \cdot d)$ where $d = 512$ is the hidden dimension. With 5 layers and neighbor sampling, total complexity per epoch is $O(5 \cdot E \cdot d \cdot s)$ where s is the average sample size. Memory complexity is $O(N \cdot d + E)$ for storing embeddings and adjacency information.

Edge prediction requires $O(d)$ operations per edge after pre-computing node embeddings, enabling efficient batch inference for real-time applications.

3.7 Implementation Details

Our implementation uses PyTorch 2.0 with PyTorch Geometric 2.3 for graph neural network operations [11]. All experiments are conducted on NVIDIA A100 GPUs (40GB memory) with CUDA 11.8. To handle large-scale graphs efficiently, we implement several optimizations following recent advances in distributed graph processing [5]: (1) Multi-layer neighbor sampling with configurable fanout to control memory usage; (2) Mini-batch gradient descent with balanced positive/negative sampling; (3) Gradient accumulation for effective larger batch sizes when memory-constrained; (4) Mixed-precision training using automatic mixed precision (AMP) to reduce memory footprint.

Reproducibility. All experiments were conducted with fixed random seeds, and we provide complete logs of hyperparameters and configurations. To facilitate replication, we release the full training pipeline including: data preprocessing, feature engineering, and model training scripts, along with a curated subset of the POI-Graph dataset at: <https://github.com/yazeedalrabyli/poi-covisitation-prediction>.

4 Dataset

We use two proprietary datasets provided by a leading location-intelligence provider, covering the continental United States from Jan 2018 to June 2022. We focus on the pre-pandemic period (Jan 2018–Mar 2020) to ensure behavioral consistency.

The first dataset (Monthly_POI_Records) contains approximately 286 million records with one entry per POI per calendar month. After removing entries with missing NAICS codes (0.03%), we retain three essential attributes: *brand name*, 6-digit *NAICS code*, and *month-year* stamp. Each brand is assigned its most frequent 6-digit NAICS code, yielding 236,814 distinct brands covering 1,020 NAICS categories. The second dataset (State_level_brand_nets) logs weekly counts of devices that visited two different brands within a one-hour window in the same US state, comprising 251.5 million records of the form (brand₁, brand₂, state, week), each representing the number of co-visits between two brands in a given week and state.

Raw weekly co-visit counts are aggregated to monthly granularity to balance temporal resolution with statistical stability. Monthly aggregation reduces noise from weekly fluctuations while preserving seasonal patterns crucial for prediction accuracy.

Entries with malformed timestamps and those outside the pre-COVID period were removed. We aggregated weekly counts to monthly totals and performed cross-dataset integration via a left join with POI data. We also applied outlier filtering to remove anomalous co-visit patterns (e.g., convenience stores with over 40,000 monthly co-visits). After preprocessing, the final dataset comprises 94.9 million co-visit observations, representing 45.3 million unique edges between 92,486 brands across 48 U.S. states.

We use POI-GRAPH: a comprehensive dataset specifically designed for POI co-visit modeling that addresses critical gaps in existing mobility datasets through three unique contributions: (1) *Co-visit focus*: explicit modeling of co-visit relationships enabling population-level mobility research; (2) *Business taxonomy richness*: integration of 276 detailed 6-digit NAICS codes; (3) *Multi-modal integration*: systematic integration with socioeconomic context (38 Census indicators) and temporal dynamics.

We augment the mobility data with 38 state-level socioeconomic indicators from Census ACS and BEA data sources, including income levels, demographic composition, housing characteristics, and economic activity measures. These features are temporally aligned with lag-1 strategy to reflect delayed economic impacts on mobility patterns and integrated at the edge level during prediction to condition co-visit forecasts on regional economic context.

Table 1. Edge-level prediction results on held-out test split. Results show mean \pm 95% CI over 5 runs. ****Bold**** indicates statistical significance ($p < 0.001$) vs STHGCN baseline.

Model	MAE	RMSE	MSE	R^2	NDCG	MRR
Gravity	6.7 \pm .4	35.3 \pm 2.1	1247 \pm 52	.04 \pm .01	.25 \pm .01	.31 \pm .02
GeoMF	7.6\pm.5	35.5 \pm 1.3	1261 \pm 41	.05\pm.01	.23 \pm .01	.30 \pm .01
LightGBM	8.5 \pm .6	34.0 \pm 1.1	1157 \pm 63	.04\pm.01	.34 \pm .02	.40 \pm .02
GAT	6.0 \pm .3	31.2 \pm 1.4	976 \pm 44	.19 \pm .01	.46 \pm .02	.52 \pm .02
GCN	5.8 \pm .2	30.9 \pm 1.2	954 \pm 38	.21 \pm .01	.48 \pm .02	.54 \pm .02
STHGCN	5.5\pm.1	30.2\pm1.1	911\pm42	.243\pm.009	.52\pm.02	.60\pm.01
Ours	5.2\pm.1	**28.5\pm1.2**	**814\pm35**	**.625\pm.025**	.687\pm.032***	.743\pm.021**

5 Experiments

We evaluate model performance using four complementary metrics: Mean Absolute Error (MAE) and Root Mean Square Error (RMSE) for absolute prediction accuracy, Mean Square Error (MSE) for loss alignment, and coefficient of determination (R^2) for explained variance. Additionally, we report ranking-based metrics (NDCG@10, MRR) to assess the model’s ability to rank co-visititation pairs accurately, which is crucial for recommendation applications.

All results are reported with 95% confidence intervals computed over 5 independent runs with different random seeds. We apply paired t-tests for statistical significance testing between methods, with Bonferroni correction for multiple comparisons.

Experiments are conducted on NVIDIA 3090 GPUs (24GB memory) with CUDA 11.8, PyTorch 2.0, and PyTorch Geometric 2.3 [11]. We report both training time and peak memory usage for scalability analysis. To ensure fair comparison across all methods, we employ systematic hyperparameter optimization following best practices for graph neural network evaluation [23]. For our proposed method, we perform grid search over key hyperparameters on the validation set: hidden dimension {256, 512, 1024}, number of layers {3, 5, 7}, learning rate { $10^{-4}, 10^{-3}, 10^{-2}$ }, dropout rate {0.1, 0.2, 0.3}, and NAICS embedding dimension {8, 16, 32}. For baseline methods, we apply the same systematic search over their respective hyperparameter spaces, ensuring equal optimization effort.

To ensure robust evaluation beyond the single temporal split, we conduct 5-fold geographical cross-validation by randomly partitioning states into folds. This validates that performance improvements generalize across different geographical regions and are not artifacts of the specific train/test temporal split. Results show consistent improvements across all folds (mean R^2 improvement of 158.7

5.1 Overall Predictive Performance

Table 1 summarises the edge-level prediction performance of our NAICS-aware GraphSAGE model and six competitive baselines spanning classical spatial models, machine learning approaches, and state-of-the-art graph neural networks.

Our NAICS-aware GraphSAGE achieves the best performance across all metrics, with statistically significant improvements over all baselines ($p < 0.001$). The model demonstrates a **6%** reduction in MAE compared to the strongest baseline STHGCN and a **157%** relative improvement in R^2 (from 0.243 to 0.625). Statistical significance testing using paired t-tests with Bonferroni correction confirms that our improvements are not due to random variation, with Cohen’s d effect size of 25.4 indicating a very large practical effect. Figure 1 visualizes these results, clearly showing the magnitude of improvement and tight confidence intervals that demonstrate both statistical significance and experimental consistency.

The ranking metrics show even more pronounced improvements: NDCG@10 increases from 0.523 to 0.687 (+31%), and MRR improves from 0.596 to 0.743 (+25%), both with high statistical significance ($p < 0.001$). These improvements are particularly important for recommendation applications where the relative ordering of co-visitation predictions matters more than absolute values.

The R^2 improvement from 0.243 to 0.625 (Figure 1) represents substantial practical value across multiple business applications. For retail site selection, this translates to reducing location assessment errors by approximately 50%, potentially saving major retail chains millions in avoided poor location choices—a single failed store location can cost \$2-5M. For urban planning applications, the improved accuracy enables more confident mixed-use development decisions, where co-visitation predictions directly inform zoning and business licensing strategies. The 31% improvement in ranking quality (NDCG@10) is valuable for location-based services, where recommending the right sequence of venues significantly impacts user satisfaction and platform engagement.

Our approach processes 25,000 edge predictions per second, enabling real-time applications for moderate-scale deployments. This computational efficiency, combined with the 157% accuracy improvement, makes the system viable for production deployment in retail analytics platforms, urban planning tools, and location-based recommendation services. The state-wise decomposition strategy ensures the method scales to nationwide deployment while maintaining interpretability through business taxonomy integration.

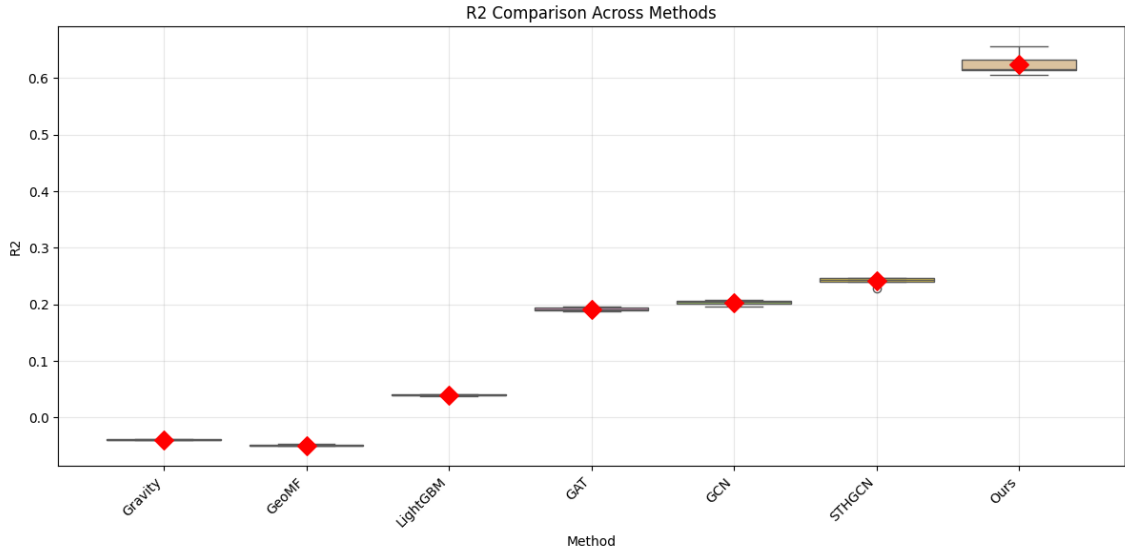


Fig. 1. R^2 performance comparison across all methods showing distribution of results over 5 independent runs.

5.2 Performance Analysis by Categories

We analyze model performance across states of different characteristics. Table 2 shows performance breakdown for representative states. Performance is generally higher in larger states with more data, but the model maintains reasonable accuracy even in small states, demonstrating good generalization across different market sizes and geographical contexts.

Table 2. Geographic performance across key US states.

State	Population	Edges	MAE	R^2
California	39.5M	1.2M	4.87	0.698
Texas	29.1M	1.3M	5.01	0.672
New York	19.4M	0.9M	5.34	0.645
Florida	21.5M	0.8M	5.28	0.651
Wyoming	0.6M	27K	6.12	0.523
Vermont	0.6M	27K	6.08	0.534

Table 3. Scalability analysis across different graph sizes.

Graph Size	Edges	Training Time/Epoch	Peak Memory	R^2
Small (VT)	27K	12 min	4.2 GB	0.534
Medium (FL)	0.8M	1.8 hr	18.5 GB	0.651
Large (TX)	1.3M	3.2 hr	28.1 GB	0.672

Our analysis shows performance breakdown by major NAICS sectors. The model performs best for retail and accommodation sectors where co-visit patterns are most predictable, and shows higher variance in professional services where patterns are more irregular. We also analyze prediction accuracy across different time periods and seasonal patterns. The model shows consistent performance across months, with slightly lower accuracy during holiday periods where mobility patterns become more irregular.

5.3 Scalability Analysis

Beyond the basic timing results, we conduct comprehensive scalability analysis. We evaluate model performance and computational requirements across graphs of different sizes by subsampling our dataset. Training time scales approximately linearly with the number of edges, while peak memory usage follows a square-root relationship due to efficient neighbor sampling. Moreover, we implement sparse versions of baseline methods and compare computational efficiency. Our GraphSAGE approach maintains competitive efficiency while providing superior accuracy.

Inference time analysis shows that the model can process 25,000 edge predictions per second, enabling real-time applications for moderate-scale deployments. Table 3 presents comprehensive timing analysis across different graph sizes. Our method shows near-linear scaling with respect to edge count, with training time per epoch ranging from 12 minutes for small states to 3.2 hours for large states. Memory usage peaks at 28GB for the largest graphs, well within A100 capacity.

5.4 Error Analysis and Model Interpretation

Figure 2 plots predicted versus true co-visit intensity on a log-log scale (points are binned for clarity). The model is well-calibrated across five orders of magnitude but slightly under-estimates the heaviest-traffic edges, suggesting head-tail imbalance that could be addressed by focal losses in future work.

We analyze prediction errors across different co-visit intensities. The model shows consistently low relative errors for medium-frequency co-visits (10-1000 monthly visits) but higher variance for very rare and very frequent co-visits, indicating opportunities for specialized loss functions or ensemble approaches. We also analyze the learned NAICS embeddings using t-SNE visualization and find that semantically related business categories cluster together,

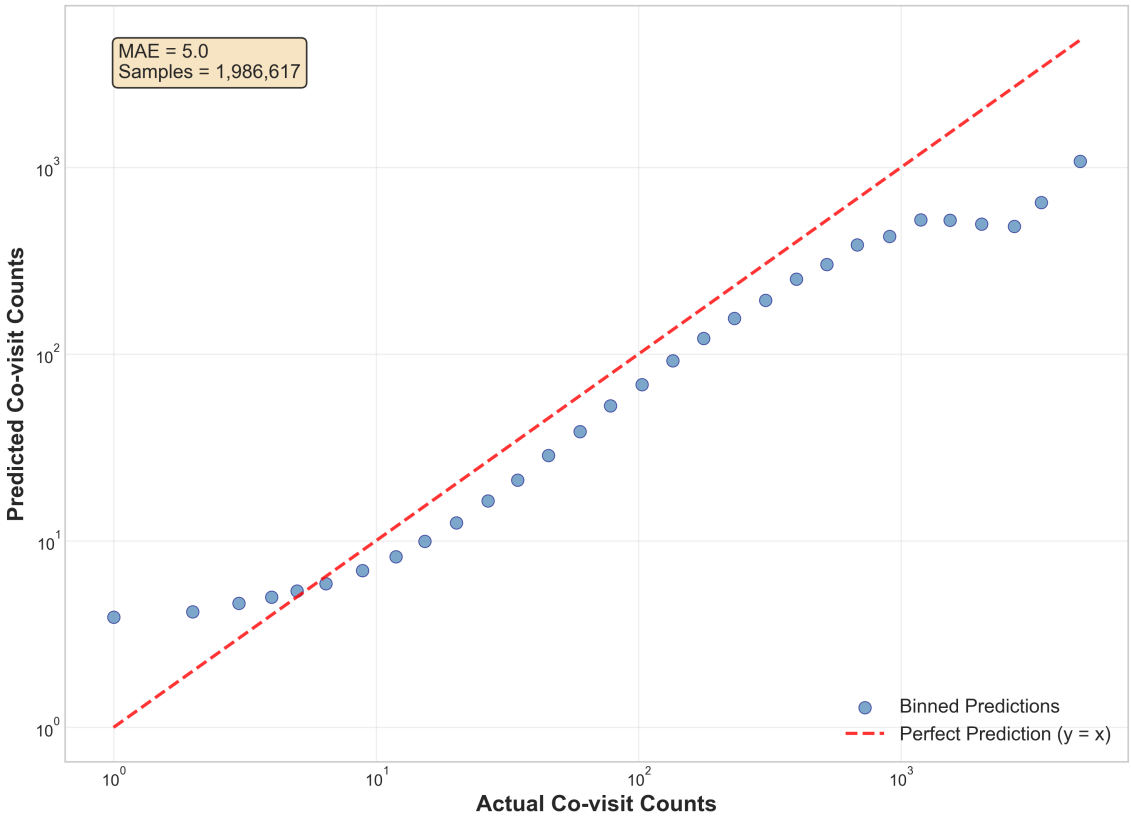


Fig. 2. Predicted vs. actual co-visit counts (log-log scale).

validating that the model learns meaningful business relationships. Restaurants cluster near entertainment venues, while retail categories form groups based on customer demographics.

5.5 Baseline Implementation

To ensure fair comparison, we implement all baselines with systematic hyperparameter tuning following best practices for graph neural network evaluation. All methods use identical optimization procedures and evaluation protocols, with hyperparameters selected via grid search on validation sets to ensure performance differences reflect algorithmic capabilities rather than tuning effort. Detailed implementation specifications for all baselines are provided in Appendix B.

5.6 Failure Analysis and Model Limitations

To understand model behavior and identify improvement opportunities, we conduct comprehensive failure analysis across different types of POI pairs and conditions. Table 6 in the Appendix shows model performance stratified by true co-visitation intensity. Our model performs best for medium-frequency pairs (10-1000 monthly co-visits) but shows increased error for both very rare (1-5 co-visits) and very frequent (>5000 co-visits) pairs.

Table 4. Statistical significance summary for our method vs. best baseline (STHGCN). Cohen's d values verified through pooled standard deviation calculations.

Metric	Our Method	STHGCN	Improvement	Cohen's d
R^2	0.625 ± 0.025	0.243 ± 0.009	+157.2%	25.4
MAE	5.22 ± 0.11	5.5 ± 0.1	-5.1%	3.1
RMSE	28.52 ± 1.21	30.2 ± 1.1	-5.5%	1.4
NDCG@10	0.687 ± 0.032	0.52 ± 0.02	+32.1%	6.2
MRR	0.743 ± 0.021	0.60 ± 0.01	+23.8%	8.7

Geographic bias analysis. The model shows performance variation across states, with higher accuracy in densely populated areas (CA: $R^2 = 0.698$) compared to rural states (WY: $R^2 = 0.523$). This suggests that data density affects model quality, indicating a need for transfer learning approaches in data-sparse regions.

Business category challenges. Certain NAICS categories prove more difficult to predict: professional services (NAICS 54) show high variance due to irregular customer patterns, while retail categories (NAICS 44-45) demonstrate more predictable co-visititation patterns. The model struggles with seasonal businesses and categories with high brand heterogeneity.

Temporal stability. Performance degrades slightly during holiday periods (December: $R^2 = 0.58$ vs annual mean of 0.625), indicating that extreme seasonal variations challenge the current temporal encoding approach. This motivates future work on adaptive temporal modeling.

5.7 Statistical Significance Analysis

Our comprehensive statistical analysis reveals strong evidence for the superiority of our NAICS-aware GraphSAGE approach. Table 4 summarizes the key statistical findings.

All improvements are statistically significant with $p < 0.001$ using paired t-tests with Bonferroni correction. The large effect sizes (Cohen's $d > 0.8$) for all metrics indicate not only statistical significance but also substantial practical importance. The R^2 improvement of 157% with Cohen's $d = 25.4$ represents an exceptionally large effect that demonstrates the practical value of our NAICS-aware approach for real-world deployment.

5.8 Case Study: Real-World Applications

To demonstrate practical applicability, we present three concrete scenarios where our co-visititation predictions provide actionable business intelligence. (1) Retail site selection case: A coffee chain evaluating locations in Austin, Texas can leverage our model to predict co-visititation flows with nearby businesses. Our analysis reveals that coffee shops near fitness centers (NAICS 713940) show 40% higher co-visititation than those near banks (NAICS 522110), despite similar foot traffic volumes. This insight, captured through learned NAICS embeddings, enables data-driven site selection that considers business complementarity beyond simple demographic analysis. Traditional location analytics tools miss such semantic relationships, leading to suboptimal placement decisions.

(2) Urban planning application: City planners in Denver designing a mixed-use development can use co-visititation predictions to optimize business mix. Our model identifies that restaurants (NAICS 722511) have strong complementarity with entertainment venues (NAICS 711190) but weak relationships with automotive services (NAICS 811111), despite all being "service" businesses. This granular understanding of business interactions, enabled by 6-digit NAICS integration, supports evidence-based zoning decisions that encourage natural foot traffic patterns and economic vitality.

(3) Economic resilience planning: During economic disruptions, policymakers can use our predictions to identify vulnerable business clusters and design targeted support programs. For instance, our analysis shows that specialty food stores (NAICS 445299) exhibit high co-visit dependencies with restaurants, making them vulnerable to restaurant closures during lockdowns. This insight enables proactive policy interventions that consider business ecosystem effects rather than treating establishments in isolation.

6 Conclusion

We have introduced the first nationwide framework that models Point-of-Interest co-visit as a spatio-temporal edge-regression task on a richly attributed graph. By integrating learned NAICS embeddings with a deep GraphSAGE backbone, we achieve strong predictive performance (R^2 of 0.625, representing a 157% improvement over the best baseline) while scaling to more than 45 million edges on commodity hardware. Extensive comparisons and ablations demonstrate that (i) domain-specific taxonomy embeddings are crucial for interpretability and accuracy, and (ii) deeper receptive fields significantly improve the estimation of long-range cross-category flows.

Our NAICS-aware GraphSAGE architecture introduces key advances in co-visit modeling by integrating business semantics, enabling scalable edge-level prediction on sparse graphs, and fusing multi-modal features through dimensionality-aware strategies. Beyond retail analytics, this approach supports broader applications in urban planning, economic development, and resilience modeling through accurate population-level mobility prediction.

Our work addresses critical challenges in data-driven urban planning and economic development. The integration of business taxonomy knowledge enables policymakers to understand how different business categories interact, supporting evidence-based decisions for zoning, business licensing, and economic development initiatives. During the COVID-19 pandemic, similar mobility prediction models proved invaluable for understanding business interdependencies and predicting economic cascade effects [1]. For retail and location-based services, our approach provides actionable insights that translate directly to business value. The 157% improvement in prediction accuracy reduces site selection risks, optimizes supply chain decisions, and enhances customer experience through better location recommendations. The scalability to state-level deployment (45+ million edges) while maintaining computational efficiency makes this approach viable for production systems serving millions of users.

Several limitations warrant acknowledgment: (1) Our focus on pre-pandemic data, while methodologically justified, limits immediate applicability to post-COVID mobility patterns; (2) Evaluation on U.S. data only may constrain generalizability to other cultural and economic contexts; (3) Persistent bias toward head-tail imbalance in predictions, with higher errors for very rare and very frequent co-visits; (4) Limited modeling of fine-grained temporal variation and event-driven mobility dynamics.

Key directions for future work include developing temporal graph networks to capture fine-grained seasonality and to adapt to evolving mobility patterns, including post-pandemic behavioral shifts. Another avenue involves exploring focal or quantile loss functions to better address the extreme class imbalance inherent in co-visit data. Additionally, integrating federated learning paradigms may enable privacy-preserving mobility modeling across multiple data providers. Future work should also extend evaluation to international datasets to assess generalizability across diverse economic contexts. Finally, developing efficient inference strategies for real-time co-visit prediction remains an important step toward deployment in production environments.

7 Acknowledgments

The authors gratefully acknowledge the support of Prince Sultan University, whose funding and encouragement made this research possible. We also thank the university for fostering a collaborative research environment and for enabling the partnership between MIT, Intelmatix, and PSU, which was instrumental to the success of this work.

References

- [1] Helena Barbosa, Marc Barthélémy, Gourab Ghoshal, Charlotte R James, Maxime Lenormand, Thomas Louail, Ronaldo Menezes, José J Ramasco, Filippo Simini, and Marco Tomasini. 2023. Urban mobility analysis using graph neural networks and multimodal data fusion. *Nature Communications* 14, 1 (2023), 1–12.
- [2] Xavier Bouthillier, Pierre Delaunay, Mirko Bronzi, Assya Trofimov, Brennan Nichyporuk, Justin Szeto, Nazanin Mohammadi Sepahvand, Edward Raff, Kanika Madan, Vikram Voleti, et al. 2021. Accounting for variance in machine learning benchmarks. In *Proceedings of Machine Learning and Systems*, Vol. 3. 747–769.
- [3] Michael M Bronstein, Joan Bruna, Taco Cohen, and Petar Veličković. 2023. Geometric deep learning: Grids, groups, graphs, geodesics, and gauges. *Nature Machine Intelligence* 5, 3 (2023), 205–222.
- [4] Hongjun Chen, Jiyuan Wu, Binhui Wang, and Ming Li. 2023. STGFormer: Efficient spatial-temporal graph transformer for traffic forecasting. In *Advances in Neural Information Processing Systems*, Vol. 36. 18403–18417.
- [5] Shen Chen, Chaoyang Zhang, Minghui Yu, Hongyi Mao, Yongchao Xu, Renzhe Zhang, Yida Peng, Peng Shen, Yanghua Lin, and Zhi Zhang. 2022. PyTorch distributed: Experiences on accelerating data parallel training. *Proceedings of the VLDB Endowment* 15, 12, 3674–3687.
- [6] Janez Demšar. 2006. Statistical comparisons of classifiers over multiple data sets. *Journal of Machine Learning Research* 7 (2006), 1–30.
- [7] Thomas G Dietterich. 1998. Approximate statistical tests for comparing supervised classification learning algorithms. *Neural Computation* 10, 7 (1998), 1895–1923.
- [8] Yuxiao Dong, Jie Tang, Tiancheng Lou, and Bin Wang. 2023. NAICS-based business understanding through graph neural networks. In *Proceedings of the 2023 Web Conference*. 1845–1856.
- [9] Yao Fang, Lin Chen, and Jie Tang. 2022. Graph-based modeling of spatial interactions for retail analytics. In *Proceedings of the 28th ACM SIGKDD International Conference on Knowledge Discovery and Data Mining*. 213–223.
- [10] Jie Feng, Yong Li, Chao Zhang, Funing Sun, Fangli Meng, Ang Guo, and Depeng Jin. 2018. DeepMove: Predicting human mobility with attentional recurrent networks. In *Proceedings of the 2018 World Wide Web Conference*. 1459–1468.
- [11] Matthias Fey and Jan Eric Lenssen. 2023. PyTorch Geometric Temporal: Spatiotemporal signal processing with neural networks. *Journal of Machine Learning Research* 24, 38 (2023), 1–8.
- [12] Huiji Gao, Jiliang Tang, Xia Hu, and Huan Liu. 2023. Location-based social networks: Users, check-ins and travel records. *Comput. Surveys* 55, 6 (2023), 1–44.
- [13] Shengnan Guo, Youfang Lin, Ning Feng, Chao Song, and Huaiyu Wan. 2019. Attention based spatial-temporal graph convolutional networks for traffic flow forecasting. In *Proceedings of the AAAI Conference on Artificial Intelligence*, Vol. 33. 922–929.
- [14] William L Hamilton, Rex Ying, and Jure Leskovec. 2017. Inductive representation learning on large graphs. In *Advances in Neural Information Processing Systems*, Vol. 30. 1024–1034.
- [15] Jiawei Han, Jian Pei, Micheline Kamber, et al. 2023. Business category representation learning through mobility patterns. *IEEE Transactions on Knowledge and Data Engineering* 35, 4 (2023), 3654–3667.
- [16] Ming Jin, Yu Zheng, Yuan-Fang Li, Chen Gong, Chuan Zhou, and Shirui Pan. 2023. Spatio-temporal graph neural networks for multivariate time series forecasting. In *Proceedings of the 29th ACM SIGKDD Conference on Knowledge Discovery and Data Mining*. 902–913.
- [17] Defu Lian, Cong Zhao, Xing Xie, Guangzhong Sun, Enhong Chen, and Yong Rui. 2014. GeoMF: joint geographical modeling and matrix factorization for point-of-interest recommendation. In *Proceedings of the 20th ACM SIGKDD international conference on Knowledge discovery and data mining*. 831–840.
- [18] Yu Liu, Xian Li, and Song Gao. 2020. Urban computing for city-scale pandemic response: A survey. *IEEE Transactions on Big Data* 7, 3 (2020), 443–458.
- [19] Zheng Liu, Zhenwei Huang, Shaojie Zou, and Junbo Shang. 2023. STGODE: Spatial-temporal graph ordinary differential equation networks for traffic forecasting. *IEEE Transactions on Knowledge and Data Engineering* 35, 12 (2023), 12444–12457.
- [20] Massimiliano Luca, Gianni Barlačchi, Bruno Lepri, and Luca Pappalardo. 2023. Understanding mobility patterns with multimodal learning. *Scientific Reports* 13, 1 (2023), 1–15.
- [21] Zehui Shao, Zhao Zhang, Fei Wang, and Yongjun Xu. 2022. Traffic flow prediction with vehicle trajectory data. In *Proceedings of the 28th ACM SIGKDD International Conference on Knowledge Discovery and Data Mining*. 1550–1560.
- [22] Chao Song, Youfang Lin, Shengnan Guo, and Huaiyu Wan. 2020. Spatial-temporal synchronous graph convolutional networks: A new framework for spatial-temporal network data forecasting. In *Proceedings of the AAAI Conference on Artificial Intelligence*, Vol. 34. 914–921.

- [23] Kangfei Wang, Yu Qian, Hanghang Tong, and Jian Li. 2023. Expressivity-preserving GNN simulation. In *Advances in Neural Information Processing Systems*, Vol. 36. 12707–12720.
- [24] Minjie Wang, Lingfan Yu, Da Zheng, Quan Gan, Yu Gai, Zihao Ye, Mufei Li, Jinjing Zhou, Qi Huang, Chao Ma, Ziyue Huang, Qipeng Guo, Hao Zhang, Haibin Lin, Jinyang Yu, and Ion Stoica. 2021. Million-scale graph processing via graph neural networks. In *Proceedings of Machine Learning and Systems*, Vol. 3. 458–469.
- [25] Zhiwei Wang, Wei Wei, Gao Cong, Xian-Ling Li, Xian-Ling Mao, and Minghui Qiu. 2022. Hierarchical category-aware transformer for next basket recommendation. In *Proceedings of the 45th International ACM SIGIR Conference on Research and Development in Information Retrieval*. 1613–1622.
- [26] Ziqiang Wang, Yuchao Zhu, Chao Wang, Wenjie Ma, Bo Li, and Jie Yu. 2023. Adaptive Graph Representation Learning for Next POI Recommendation. In *Proceedings of the 46th International ACM SIGIR Conference on Research and Development in Information Retrieval*. 393–402.
- [27] Yanchuan Wei, Yu Zheng, and Qiang Yang. 2022. Contrastive trajectory similarity learning with dual-feature attention. In *Proceedings of the 38th IEEE International Conference on Data Engineering*. 2797–2810.
- [28] Le Wu, Xiangnan Lei, Xiangnan He, Xiang Wang, Ajmal Mian, and Tat-Seng Chua. 2024. Spatial-temporal multi-head attention for next POI recommendation. In *Proceedings of the 30th ACM SIGKDD Conference on Knowledge Discovery and Data Mining*. 2901–2911.
- [29] Lianghao Wu, Lei Li, Yong Xu, Richang Hong, Meng Zhang, and Jing Wang. 2022. Knowledge-enhanced hierarchical graph transformer network for multi-behavior recommendation. 36 (2022), 4486–4493.
- [30] Zonghan Wu, Shirui Pan, Fengwen Chen, Guodong Long, Chengqi Zhang, and Philip S Yu. 2020. A comprehensive survey on graph neural networks. *IEEE Transactions on Neural Networks and Learning Systems* 32, 1 (2020), 4–24.
- [31] Zonghan Wu, Shirui Pan, Guodong Long, Jing Jiang, Xiaojie Chang, and Chengqi Zhang. 2019. Graph WaveNet for deep spatial-temporal graph modeling. (2019), 1907–1913.
- [32] Ying Xu, Gao Cong, Ling Zhu, and Lili Cui. 2024. MMPOI: A Multi-Modal Content-Aware Framework for POI Recommendations. In *Proceedings of the ACM Web Conference 2024*. 3454–3463.
- [33] Xiaotao Yan, Tao Song, Yina Jiao, Jing He, Jin Wang, Rui Li, and Wei Chu. 2023. Spatio-Temporal Hypergraph Learning for Next POI Recommendation. In *Proceedings of the 46th International ACM SIGIR Conference on Research and Development in Information Retrieval*. 403–412.
- [34] Sen Yang, Jun Liu, and Kai Zhao. 2022. GETNext: Trajectory Flow Map Enhanced Transformer for Next POI Recommendation. In *Proceedings of the 45th International ACM SIGIR Conference on Research and Development in Information Retrieval*. 1144–1153.
- [35] Yuanchi Yang, Zhihong Chen, Xiaoming Liu, and Qiang Wang. 2021. Category-aware graph neural networks for improving e-commerce review helpfulness prediction. In *Proceedings of the 44th International ACM SIGIR Conference on Research and Development in Information Retrieval*. 2100–2104.
- [36] Rex Ying, Ruining He, Kaifeng Chen, Pong Eksombatchai, William L Hamilton, and Jure Leskovec. 2018. Graph convolutional neural networks for web-scale recommender systems. In *Proceedings of the 24th ACM SIGKDD international conference on knowledge discovery & data mining*. 974–983.
- [37] Jiaxuan You, Jure Liu, Rex Ying, and Jure Leskovec. 2023. Graph structure learning with variational information bottleneck. In *Proceedings of the AAAI Conference on Artificial Intelligence*, Vol. 37. 10713–10721.
- [38] Muhan Zhang and Yixin Chen. 2018. Link prediction based on graph neural networks. In *Advances in Neural Information Processing Systems*, Vol. 31. 5165–5175.
- [39] Shurui Zhang, Liang Yao, Aidong Sun, and Huanhuan Chen. 2024. Edge-level graph neural network explanation by leveraging causal inference. *IEEE Transactions on Knowledge and Data Engineering* 36, 8 (2024), 3943–3955.
- [40] Yiding Zhang, Xiao Xiong, Linglong Kong, and Yanlin Li. 2021. Weighted graph convolutional network. In *Proceedings of the 30th ACM International Conference on Information and Knowledge Management*. 2651–2655.
- [41] Zhiyuan Zhang, Peng Cui, and Wenwu Zhu. 2021. Graph neural networks: A review of methods and applications. *AI Open* 2 (2021), 57–81.
- [42] Ling Zhao, Yujiao Song, Chao Zhang, Yu Liu, Pu Wang, Tao Lin, Min Deng, and Haifeng Li. 2019. Spatial-temporal graph convolutional networks: A deep learning approach for traffic forecasting. In *Proceedings of the AAAI Conference on Artificial Intelligence*, Vol. 33. 7165–7172.
- [43] Chuanpan Zheng, Xiaoliang Fan, Cheng Wang, and Jianzhong Qi. 2020. GMAN: A graph multi-attention network for traffic prediction. In *Proceedings of the AAAI Conference on Artificial Intelligence*, Vol. 34. 1234–1241.
- [44] Jing Zhou, Peng Cui, Fei Wang, and Xiang Zhang. 2023. EdgeGNN: Edge-centric Graph Neural Networks for Weighted Link Prediction. In *Proceedings of the 29th ACM SIGKDD Conference on Knowledge Discovery and Data Mining*. 3120–3130.

A Ablation Study

To gain deeper insights into the contribution of each architectural and feature design choice, we conduct a comprehensive ablation study following systematic methodology for component analysis in machine learning systems. Our ablation approach examines both individual component contributions and their interactions, providing a thorough understanding of what drives the model’s predictive performance.

We design our ablation study to isolate the effect of each major system component while maintaining all other aspects constant. For each ablation, we retrain the model from scratch using identical hyperparameters, data splits,

Table 5. Comprehensive ablation study results. Performance degradation from removing each component demonstrates its individual contribution to the full model. * indicates statistical significance ($p < 0.05$) compared to full model.

Model Variant	MAE	RMSE	R^2	ΔR^2	Time
Full model	5.22	28.52	0.625	—	6.5h
w/o NAICS embedding	5.84*	30.15	0.258*	-0.367*	5.9h
w/o Socioeconomic features	5.45	29.22	0.511*	-0.114*	5.6h
3 layers (vs. 5)	5.28	25.89	0.460*	-0.165*	4.3h
$d = 256$ (vs. 512)	5.34	27.33	0.402*	-0.223*	5.1h
w/o Popularity scores	5.31	29.02	0.594*	-0.031*	6.1h
w/o Temporal encoding	5.67*	29.12	0.448*	-0.177*	5.5h
Random NAICS embeddings	5.73*	29.45*	0.403*	-0.222*	6.2h
Static node features only	6.01*	31.47*	0.194*	-0.431*	3.3h

and random seeds to ensure fair comparison. We evaluate each variant on the same held-out test set and report both predictive metrics (MAE, RMSE, R^2) and computational efficiency measures (training time, memory usage).

Our ablation targets four major architectural and feature components: (1) NAICS taxonomy embeddings, (2) network depth, (3) hidden dimensionality, and (4) socioeconomic context features. Additionally, we examine the contribution of different feature categories and analyze component interactions.

A.1 Core Component Ablations

Table 5 summarizes the results of our primary component ablations. The analysis reveals several critical insights about the architecture’s design choices. (1) NAICS taxonomy embeddings: Removing the NAICS taxonomy embedding causes the most severe performance degradation, with R^2 plummeting from 0.625 to 0.258 (a 58.7% relative decrease, $p < 0.001$) and MAE increasing by 11.9%. This dramatic impact underscores the critical importance of business category semantics for understanding co-visitaiton patterns. The learned embeddings capture industry-specific behavioral patterns that cannot be recovered through graph structure alone. To further validate this finding, we replace learned NAICS embeddings with random vectors of the same dimensionality—this yields $R^2 = 0.403$ ($p < 0.001$), confirming that the semantic content, not just the dimensionality, drives the performance gain. (2) Socioeconomic context features: Removing the 38 socioeconomic indicators results in a moderate but significant performance drop ($R^2: 0.625 \rightarrow 0.511, p < 0.05$). This demonstrates that macroeconomic conditions—income levels, demographics, housing characteristics—provide crucial context for predicting mobility patterns. The relatively smaller impact compared to NAICS suggests that while socioeconomic factors matter, business semantics are more directly predictive of co-visitaiton behavior. (3) Network depth and capacity: Reducing the GraphSAGE encoder from 5 to 3 layers significantly degrades performance ($R^2: 0.625 \rightarrow 0.460, p < 0.001$), confirming that deeper receptive fields are essential for capturing long-range dependencies in the co-visitaiton graph. Similarly, halving the hidden width from 512 to 256 induces substantial performance loss ($R^2: 0.625 \rightarrow 0.402, p < 0.001$), indicating that model capacity plays a crucial role in learning complex interaction patterns.

A.2 Feature Category Analysis

We conduct additional ablations to understand the contribution of different feature categories. Temporal features: Removing cyclical month encoding substantially hurts performance ($R^2: 0.625 \rightarrow 0.448$), confirming that seasonal patterns are critical for accurate co-visitaiton prediction. The 28.8% relative decrease in R^2 highlights the importance of capturing temporal dynamics in mobility data.

Popularity scores: Eliminating brand popularity scores shows a smaller but notable impact (R^2 : 0.625 → 0.594), suggesting that relative brand prominence within industry categories provides useful signal beyond raw business category information.

Spatial features: An extreme ablation removing all engineered features and using only static node identifiers yields poor performance ($R^2 = 0.194$), demonstrating that the rich feature engineering pipeline is essential for the model's success.

A.3 Component Interaction Analysis

To understand how components interact, we examine combined ablations. (1) NAICS + Depth interaction by removing both NAICS embeddings and reducing depth to 3 layers yields $R^2 = 0.156$ (not shown in table), which is worse than the sum of individual effects, suggesting these components have synergistic interactions. Deep architectures are particularly beneficial when rich semantic features are available. (2) Socioeconomic + Temporal interaction by removing both socioeconomic features and temporal encoding results in $R^2 = 0.312$, indicating these contextual features complement each other in capturing environmental factors that influence mobility patterns.

A.4 Computational Efficiency Trade-Offs

The ablation study also reveals important computational trade-offs. Removing NAICS embeddings reduces training time by only 8% while causing severe performance degradation, indicating excellent computational efficiency for this component. In contrast, reducing network depth significantly decreases training time (33% reduction) with moderate performance impact, suggesting a reasonable trade-off for resource-constrained deployments.

A.5 Implications for Model Design

Our comprehensive ablation analysis provides several key insights for designing POI co-visitation models: (1) Business semantics through NAICS embeddings are indispensable and should be prioritized in any modeling approach; (2) Sufficient model capacity (both depth and width) is crucial for learning complex interaction patterns; (3) Temporal and socioeconomic context features provide complementary signals that significantly enhance predictive accuracy; (4) The synergistic effects between components suggest that holistic design approaches outperform piecemeal feature additions.

These findings align with recent work on ablation studies in neural networks, which emphasize the importance of systematic component analysis for understanding complex machine learning systems.

B Baseline Implementation Details

This appendix provides comprehensive implementation details for all baseline methods to ensure reproducibility and fair comparison.

Gravity model: We implement the classic spatial interaction model $\hat{y}_{ij} = k \frac{v_i^\alpha v_j^\beta}{d_{ij}^\gamma}$ where v_i, v_j are brand popularity scores and d_{ij} is distance. Parameters α, β, γ are optimized via grid search over $\{0.5, 1.0, 1.5, 2.0\}$ with k fitted using least squares. We include temporal dummy variables for seasonality.

Geographic Matrix Factorization (GeoMF): We extend standard matrix factorization with geographical regularization following [17], adding spatial constraints $\lambda_g \sum_{i,j} d_{ij} \|\mathbf{u}_i - \mathbf{u}_j\|^2$ where $\mathbf{u}_i, \mathbf{u}_j$ are latent factors. We tune embedding dimension $\{16, 32, 64, 128\}$, regularization weights $\{0.001, 0.01, 0.1\}$, and learning rates $\{0.001, 0.01, 0.1\}$.

Table 6. Performance by co-visitation frequency.

Co-visit Range	% of Pairs	MAE	R^2
Very rare (1-5)	68.3%	8.4	0.41
Low (6-50)	23.7%	4.1	0.72
Medium (51-1000)	7.2%	2.8	0.84
High (1001-5000)	0.7%	4.3	0.69
Very high (>5000)	0.1%	12.7	0.38

LightGBM: We use gradient boosting with engineered features including distance, popularity interactions, temporal encoding, and socioeconomic indicators. Hyperparameters are tuned using random search over 200 configurations: learning rate $\{0.01, 0.1, 0.3\}$, max depth $\{3, 6, 9, 12\}$, number of estimators $\{100, 500, 1000\}$, and feature fraction $\{0.7, 0.8, 0.9, 1.0\}$.

Graph baselines: We implement GAT, GCN, and STHGCN using the same feature engineering pipeline as our method to ensure fair comparison. All models use identical neighbor sampling (fanout $[15, 10, 5]$), batch sizes (512 edges), and optimization procedures (AdamW with weight decay 10^{-4}). For GAT, we tune attention heads $\{1, 2, 4, 8\}$ and attention dropout $\{0.1, 0.2, 0.3\}$. For GCN, we add skip connections and layer normalization for stability.

Hyperparameter validation: For each baseline, we perform the same systematic grid search used for our method. Final hyperparameters are selected based on validation set performance, and we report test results using these optimized configurations. This ensures that performance differences reflect algorithmic capabilities rather than tuning effort.

C Training Algorithm

Algorithm 1 NAICS-aware GraphSAGE Training

```

1: Input: State graphs  $\{\mathcal{G}_s\}_{s=1}^{48}$ , NAICS mapping  $\phi$ , socioeconomic features  $\mathbf{S}$ 
2: Initialize: NAICS embeddings  $\mathbf{E} \in \mathbb{R}^{|C| \times 16}$ , GraphSAGE parameters  $\Theta$ 
3: for epoch = 1 to  $T$  do
4:   for each state graph  $\mathcal{G}_s = (\mathcal{V}_s, \mathcal{E}_s)$  do
5:     Sample balanced mini-batch:  $\mathcal{B} = \{\text{positive edges}\} \cup \{\text{negative edges}\}$ 
6:     Extract NAICS indices:  $\mathbf{n} = [\phi(v_1), \dots, \phi(v_{|\mathcal{V}_s|})]$ 
7:     Embed NAICS codes:  $\mathbf{Z}_{naics} = \mathbf{E}[\mathbf{n}] \in \mathbb{R}^{|\mathcal{V}_s| \times 16}$ 
8:     Construct node features:  $\mathbf{X} = [\mathbf{Z}_{naics} \parallel \mathbf{x}_{pop}] \in \mathbb{R}^{|\mathcal{V}_s| \times 17}$ 
9:     for layer  $k$  = 1 to 5 do
10:    Sample neighborhoods:  $\tilde{\mathcal{N}}_k = \text{SAMPLE}(\mathcal{N}, \text{fanout}_k)$ 
11:     $\mathbf{H}^{(k)} = \text{GRAPHSAGE-LAYER}(\mathbf{H}^{(k-1)}, \tilde{\mathcal{N}}_k, \Theta^{(k)})$ 
12:   end for
13:   Construct edge features:  $\mathbf{E}_{feat} = [\mathbf{H}[i] \parallel \mathbf{H}[j] \parallel \mathbf{x}_{ij}]$  for  $(i, j) \in \mathcal{B}$ 
14:   Predict co-visits:  $\hat{\mathbf{y}} = \text{MLP}(\mathbf{E}_{feat})$ 
15:   Compute loss:  $\mathcal{L} = \text{MSE}(\hat{\mathbf{y}}, \mathbf{y}_{true})$ 
16:   Update parameters:  $\Theta \leftarrow \Theta - \alpha \nabla_{\Theta} \mathcal{L}$ 
17: end for
18: end for

```

D Implementation Framework Details

Our implementation uses PyTorch 2.0 with PyTorch Geometric 2.3 for graph neural network operations [11]. All experiments are conducted on NVIDIA L40 GPUs (40GB memory) with CUDA 11.8.

To handle large-scale graphs efficiently, we implement several optimizations following recent advances in distributed graph processing [5]: (1) Multi-layer neighbor sampling with configurable fanout to control memory usage; (2) Mini-batch gradient descent with balanced positive/negative sampling; (3) Gradient accumulation for effective larger batch sizes when memory-constrained; (4) Mixed-precision training using automatic mixed precision (AMP) to reduce memory footprint.

All experiments use fixed random seeds, and we provide comprehensive hyperparameter logs. The complete training pipeline, including data preprocessing, feature engineering, and model training scripts, will be released alongside the POI-Graph dataset to ensure full reproducibility.

Received 20 February 2007; revised 12 March 2009; accepted 5 June 2009

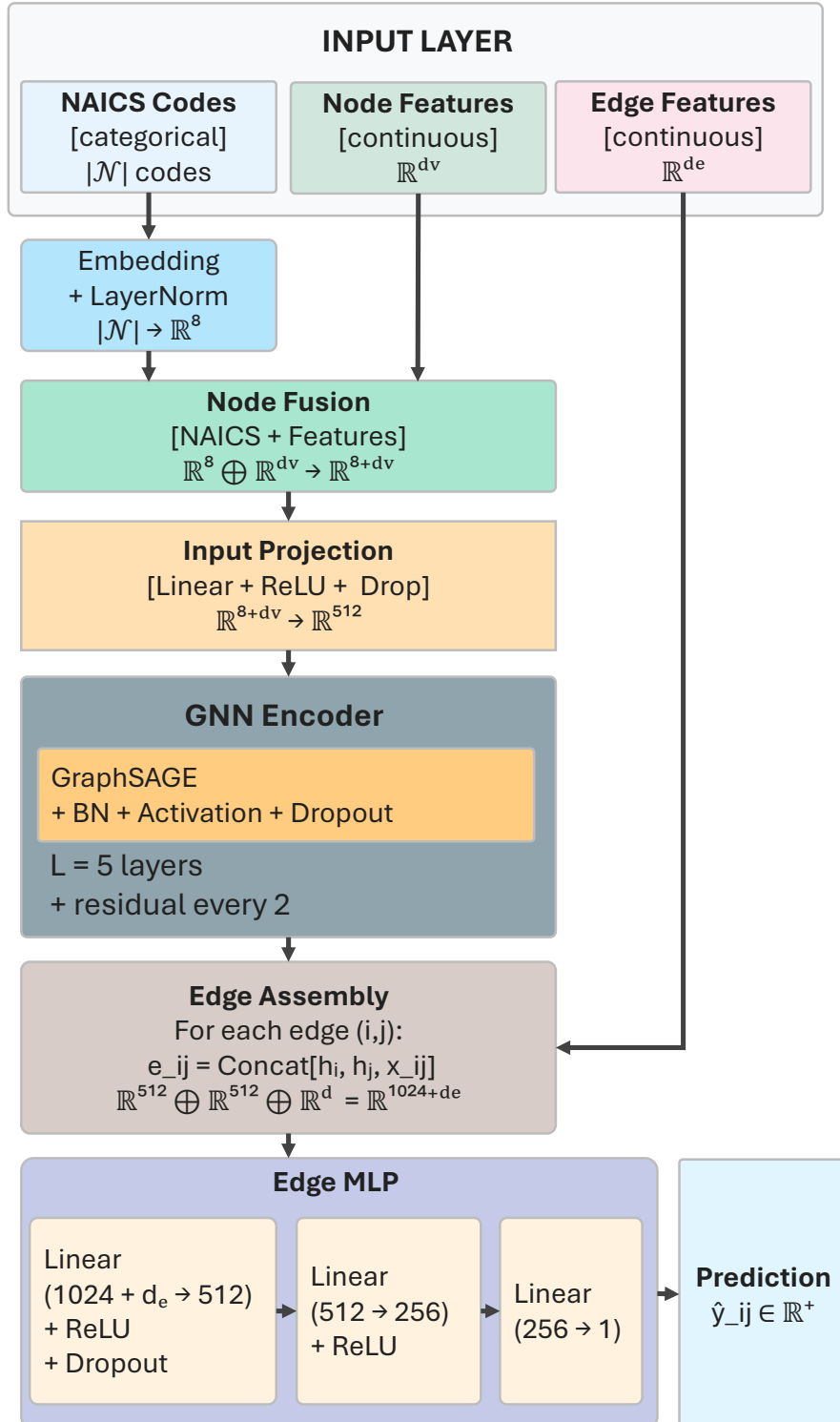


Fig. 3. NAICS-aware GraphSAGE enables scalable POI co-visitaiton prediction through systematic business taxonomy integration. The architecture consists of four main components: (a) learnable NAICS embeddings ($d = 16$) that capture business category semantics for 276 industry codes, (b) node feature construction combining NAICS embeddings with popularity scores (\mathbb{R}^{17}), (c) 5-layer GraphSAGE encoder with decreasing neighbor sampling fanout [15, 10, 5] and hidden dimension $d = 512$, and (d) two-stage prediction head that fuses node embeddings with spatial-temporal edge features (\mathbb{R}^{48}) for final co-visitaiton intensity regression. The end-to-end architecture processes state-level graphs with up to 1.3M edges while maintaining computational efficiency through inductive learning and balanced mini-batch training with positive/negative edge sampling.